

GT2011-45- %

CHARACTERIZING THE EFFECT OF RADIAL VANE HEIGHT ON FLAME MIGRATION IN AN ULTRA COMPACT COMBUSTOR

Kenneth D. LeBay
Marc D. Polanka
Richard D. Branam

Department of Aeronautics and Astronautics
Air Force Institute of Technology
WPAFB, OH, USA

ABSTRACT

The Ultra Compact Combustor (UCC) has shown viable merit for significantly improving gas turbine combustor performance. UCC models for small engines can provide centrifugal loading up to 4,000 gs. However, as the scale of the combustor increases, the g-load will necessarily decrease and the radial vane height will increase. Thus, the importance of understanding flame migration over increasing radial vane heights is pivotal to the applicability of this design to larger engine diameters. The Air Force Institute of Technology's Combustion Optimization and Analysis Laser laboratory studied this effect with a sectional UCC model using three different vane heights. By varying the mass flow rates of the circumferential UCC section, the g-loading was varied from 500-2,000 gs. Two-line Planar Laser Induced Fluorescence at 10Hz was used for 2D temperature profiles. High-speed video at 2kHz was also used for qualitative flame migration characterization. Several cases were studied varying the radial vane height, the circumferential g-load, and the UCC/core mass flow ratio but specifically focusing on the interaction between matching the core mass flow and the core freestream velocity among the different vane heights. Finally, the decreased core flow velocity for the same mass flow weakened the shear layer between the main and cavity flows and this allowed deeper flame migration into the core flow from the UCC. Control of the overall flame migration is the key to produce desirable combustor exit temperature profiles. Increased spans lead

to higher velocity gradients and increased flame injection angles at the same mass flow rates. However, at the same core flow velocities and UCC to core flow velocity ratios the flame injection angle was relatively independent of the radial vane height and almost entirely dependent on the core flow velocity alone.

Disclaimer

The views expressed in this paper are those of the authors and do not reflect the official policy or position of the United States Air Force, Department of Defense, or the United States Government.

NOMENCLATURE

A	Area
AFIT	Air Force Institute of Technology
AFRL	Air Force Research Laboratory
g	Gravitational Constant for Earth
HSV	High Speed Video
ITB	Inter-Turbine Burner
\dot{m}	Mass flow rate (kg/min)
MFR	UCC to Core Mass Flow Ratio
OH	Hydroxyl radical
PLIF	Planar Laser Induced Fluorescence
r	Radius

R	Ratio of $Q1(5)/Q1(14)$
RVC	Radial Vane Cavity
T	Temperature
V	Velocity
UCC	Ultra Compact Combustor
ϕ	Equivalence ratio
ρ	Density

INTRODUCTION

The current jet engine design trend pushes for maximum thrust and efficiency while reducing size and weight. This trend can benefit from the use of a highly compact combustor operating near or above stoichiometric conditions, with either inter or intra turbine burning [1,2]. This will lead to flame migration further and further downstream of the primary reaction zone. The main limitation to this trend is the turbine inlet flow conditions, specifically the need for a uniform temperature profile and complete combustion to avoid adverse affects on the turbine blades [3, 4]. One design seeking to meet all of the above criteria is the Ultra-Compact Combustor/Inter-Turbine Burner (UCC/ITB) currently being developed at the Air Force Research Laboratories (AFRL) [5,6] aided by the Air Force Institute of Technology (AFIT) [7].

The UCC concept is based on data collected from the Trapped Vortex Combustor [8], research on a jet swirled combustor developed by Yonezawa et. al. [9], and the research conducted by Lewis [10] on high-g flame speed. Figure 1 contains images of a conventional annular combustor (left) and the UCC (right). As shown in this figure, for the UCC the flow is directed into a circumferential cavity at high g-loading. The flame is allowed to recirculate within the circumferential cavity such that combustion can efficiently occur even in a fuel rich regime [5]. As the combustion process nears completion, buoyancy keeps the heavy incompletely burned hydrocarbons in the circumferential cavity while allowing the lighter, hot gas products to travel out of the cavity and into the main flow. This combination of high-g loading and buoyancy is believed to be a root cause of the UCC's demonstrated benefits. Previous work has included numerical investigations on the UCC-ITB [11] and on radial vane cavity geometry changes [12, 13], while experimental investigation have studied the full UCC using Laser Doppler Velocimetry [14] and a sectional model to determine the effect of g-loading [15].

The current AFRL UCC rig, shown in Figure 1, was approximately 15 cm in diameter and provided g-loading up to 4,000 g's depending on mass flow. However, a full-scale jet engine would require the UCC to be scaled up to the range of 50-75 cm in diameter. This could result in a significantly reduced circumferential g-load This scaling will also require a two to five fold increase in the radial vane height. Since the primary reaction zone is along the outer diameter of the core flow, migration of the hot exit gases is required toward the inner diameter to

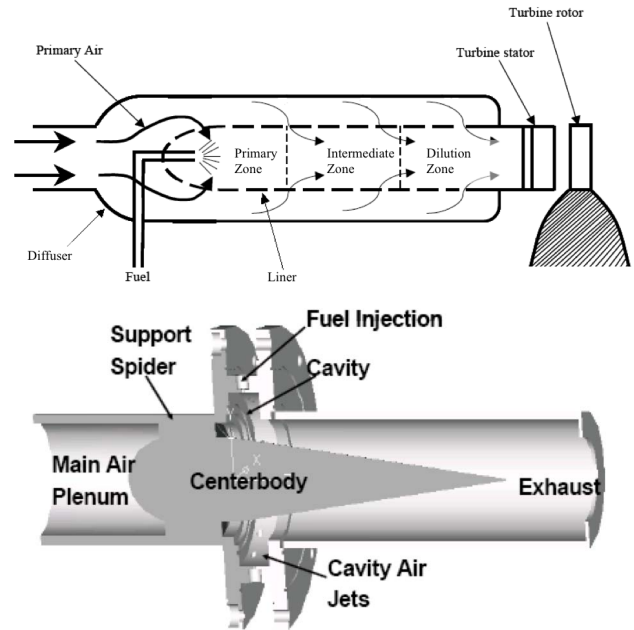


FIGURE 1. Conventional axial combustor (top) and Ultra Compact Combustor (bottom) [5]

produce a uniform temperature profile. Therefore, significantly taller vane heights might be problematic for the UCC design at the combustor-turbine interface. Thus, it was vital to choose diagnostic methods appropriate for this interface and OH-PLIF thermometry was chosen.

This investigation was also the first extensive use of simultaneous 2-line OH Planar Laser Induced Fluorescence (PLIF) thermometry to interrogate the combustor-turbine interface. While 2-line PLIF thermometry using the line-peak ratio method was proposed initially by Cattolica in 1981 [16] and extensive work on the technique was continued by Lucht in 1982 [17] and Seitzman in 1994 [18]. The first planar data was not presented until Meier in 2000 [19] and the first (and seemingly only) single-shot data by Giezendanner in 2005 [20]. However, these investigations, as well as others, have interrogated calibration flames, diffusion flames, and the primary combustor reaction zone but not the secondary reaction zone leading to the combustor-turbine interface. Inline with the previous discussion on stoichiometric combustor design trends, management of this interface is pivotal to the realization of not only the UCC but of similar next-generation combustor designs.

The objective of this research was to characterize the effect of radial vane height on flame migration. This will serve as an incremental step toward understanding the physics of high-g flame migration applied to compact combustion systems such as the UCC, where the first turbine vane is integrated into the combustor. The overarching goal is to provide a sufficient understanding

of the UCC concept for further enhancement and future implementation.

Experimental Setup

While difficult to conduct this study on AFRL's full annular rig, AFIT's Combustion Optimization and Analysis Laser (COAL) Laboratory was ideally suited for this analysis. The AFIT's UCC model (Figures 2 & 3) was derived from the AFRL model to intentionally allow the use of non-intrusive laser diagnostics and rapid testing of multiple geometric configurations. The model was constructed of 316 stainless steel and consists of two sections: the core flow section and the UCC section. The core flow section is compared to the AFRL rig in Figure 2 highlighting the location of the radial vanes of each rig. The core flow section has a channel height of 30 mm and was configured with one of three radial vanes (14 mm, 28 mm, and 56 mm). The UCC section is shown in Figure 3 mounted to the core flow section. The UCC section has a channel depth of 13.5mm, a channel width of 38mm, and a radius of curvature of 55mm. Since the radius of curvature is fixed, the g-load was changed by varying the UCC mass flow rates to produce g-loads from 500-2,000 g's. The UCC to core air mass flow ratio (MFR) was varied from 10-30%. Propane was used as the fuel for its similarities to JP-8 in heat release and fuel-to-air ratio while still producing relatively clean flames friendly to laser diagnostics. The lab's compressors provide up to 7 kg/min of air to the core flow section and up to 2 kg/min to the UCC section, both of which could be heated to 500K for improved lighting. Gaseous fuel delivery via high precision mass flow controllers provided up to 50 SLPM of Propane (C_3H_8) for the combustor.

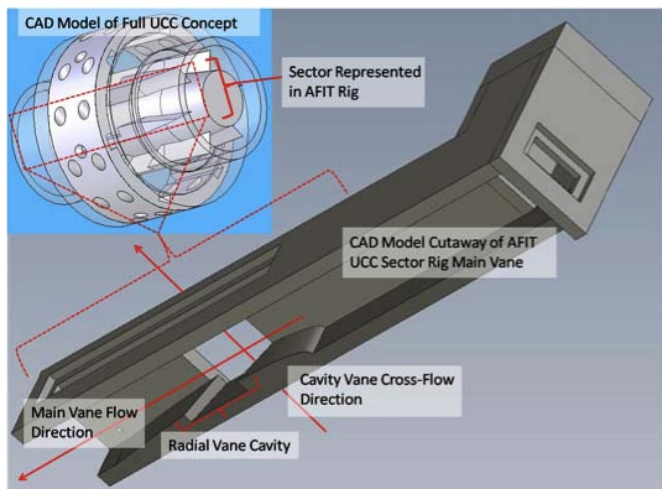


FIGURE 2. Full UCC Airfoil Location (inset) and UCC Sectional Model airfoil

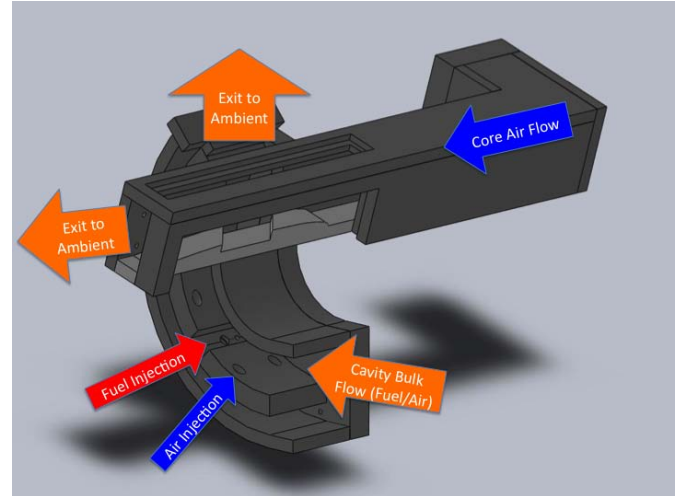


FIGURE 3. UCC Curved Section

Two-line OH Planar Laser-Induced Fluorescence (PLIF) was used to collect planar flame location and temperature data at 10Hz. The PLIF system was a custom setup designed by Innovative Scientific Solutions, Inc. and consists of a Quanta-Ray dual-pulsed Nd:YAG laser with frequency conversion unit to produce dual 532 nm pulses, two narrowband Continuum ND-6000 dye lasers with UV frequency conversion, and two Princeton Instruments PI-Max 512x512 pixel ICCD cameras with Nikkor PK-12 lens and UV filter. The PLIF thermometry technique used the intensity ratio method of two A-X(1-0) rotation-vibration transition lines [18]. The two OH transition lines interrogated were $Q_1(5)$ and $Q_1(14)$, which were excited at 282.75 nm and 286.465 nm respectively. The background was subtracted and the remaining signal was normalized with respect to incident laser power. These normalized intensities from each PLIF transition were then used as a ratio, $R=Q_1(14)/Q_1(5)$, in the input Equation 1 which was derived from calibration with a nearly adiabatic equilibrium flame from a Hencken burner.

$$T = 3333.333 * R + 901.333 \quad (1)$$

The test matrix was built to study the effect of radial vane height on the flame migration from the circumferential cavity. This matrix focused on varying the radial vane height, g-loading, cavity/main air mass flow ratio, and equivalence ratio. For a given test the cavity air and fuel mass flows were set establishing a desired cavity equivalence ratio and g-load, see Table 1. The g-load was estimated using the air mass flow, exit area, radius of curvature, and density for an equilibrium flame, per Equation 2. Then, the main air mass flow was varied to change the cavity/main air mass flow ratio. Comparisons were made between

matching the core mass flows and the core flow velocities. This alters the flow migration out of the combustion cavity. The cavity/main air mass flow ratios used were 0.1, 0.2, and 0.3. The equivalence ratio (ϕ) was held constant at $\phi = 2.0$. Figure 4 shows pictorially the data collection locations of PLIF and high-speed video, which were taken at 10 Hz with the two Princeton cameras and at 2 kHz with a color Phantom V12.1 respectively. Table 2 shows the exact locations of each data collection location along the span of each vane.

TABLE 1. Test Matrix

Test Case	Vane Height	G-Load g's	MFR	V_{core} m/s	V_{UCC}/V_{core}
1	14 mm	1000	0.1	26.2	0.887
2	14 mm	1000	0.2	13.1	1.773
3	14 mm	1000	0.3	6.55	3.456
4	28 mm	500	0.2	6.55	2.51
5	28mm	1000	0.2	6.55	3.456
6	28 mm	2000	0.2	6.55	5.02
7	28 mm	1000	0.1	13.1	1.773
8	28 mm	1000	0.3	4.464	5.203
9	28 mm	1000	0.05	26.2	0.887
10	56 mm	1000	0.1	6.55	3.456
11	56 mm	1000	0.2	3.275	7.093
12	56 mm	1000	0.3	2.182	10.645
13	56 mm	1000	0.05	13.1	1.773
14	56 mm	1000	0.025	26.2	0.887

$$g\ load = \frac{\dot{m}^2}{\rho^2 A^2 r g} \quad (2)$$

Figure 5 shows the OH-PLIF spatial calibration image showing the UCC (behind the plane) and core flow directions, the leading and trailing edges of the radial vane, the radial vane cavity, the location of exit plane interrogation, and approximate lengths of each feature. The image had a spatial calibration constant of 0.165mm/pixel yielding a 42.24 mm by 84.48 mm total image size for the 256 by 512 pixel image. Figure 6 shows a 200 image (20 sec) average of OH fluorescence signal counts before

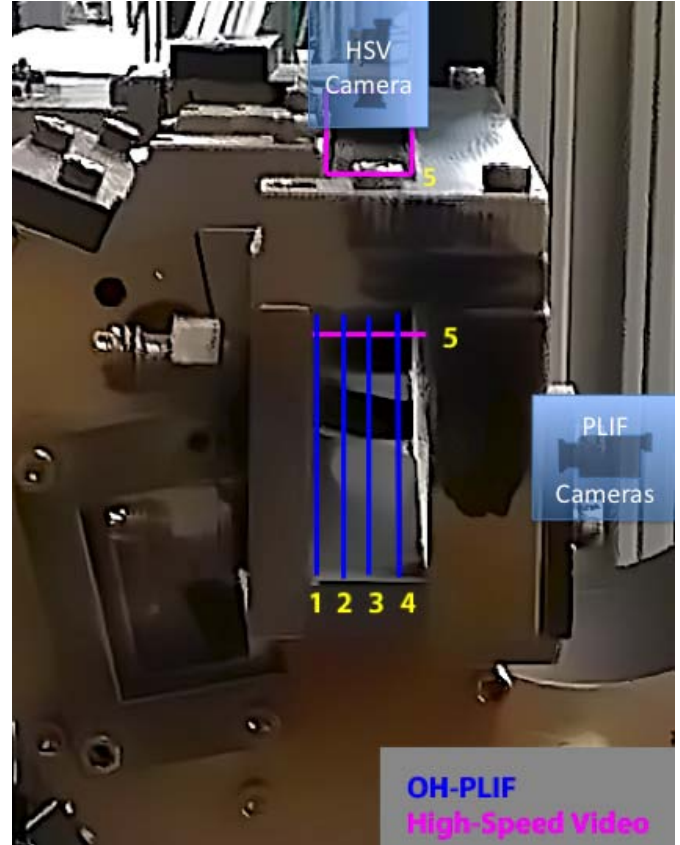


FIGURE 4. UCC Data Collection Locations

TABLE 2. Data Collection Planes (Distance from Cavity Interface)

Vane Height	Plane 1	Plane 2	Plane 3	Plane 4
14 mm	3 mm	6 mm	9 mm	
Frac. of Span	0.20	0.40	0.60	
28 mm	6 mm	12 mm	18 mm	24 mm
Frac. of Span	0.20	0.40	0.60	0.80
56 mm	6 mm	12 mm	24 mm	48 mm
Frac. of Span	0.10	0.20	0.40	0.60

the background subtraction and normalization by laser power. It is important to note that the PLIF thermometry technique inherently only yields measurements in regions of OH presence (e.g. within the flame). In Figure 6 this is indicated by the y region from approximately 3-23 mm. Outside of the flame, no OH exists and therefore no temperature is inferred.

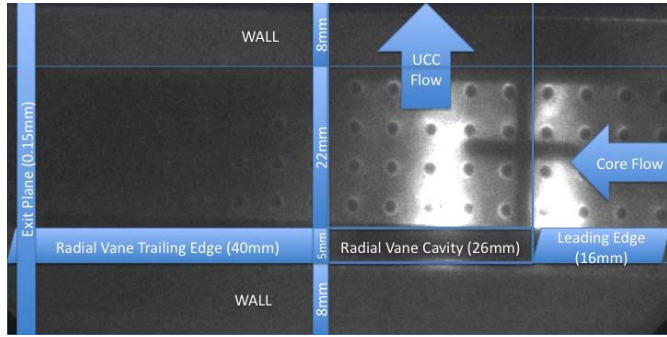


FIGURE 5. Spatial Calibration Image for OH-PLIF data collection. Rectangle indicates the location of the radial vane cavity, UCC flow, core flow, and exit plane location.

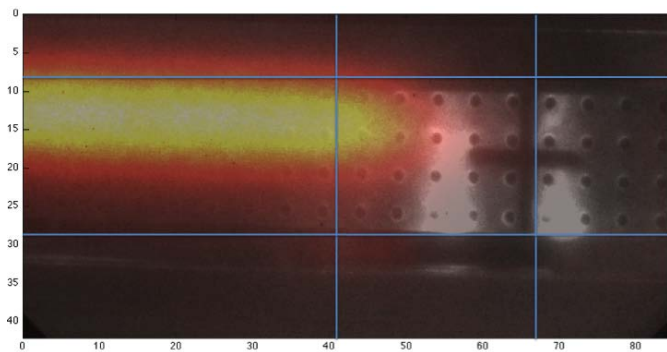


FIGURE 6. A Raw 200 Image Average of OH Fluorescence Signal Counts

RESULTS

The two-line OH-PLIF temperature measurements in the figures that follow were collected at the locations listed in Table 2 and computed from a 20 second (200 image) temporal average of OH-PLIF signal for each line. Figure 7 shows a representative data set for the baseline case (Test Case 5) where the vane height was 28 mm, the g-load was 1000, and the UCC to core air mass flow ratio (MFR) was 0.2. As indicated in these figures, the temperature continued to increase as the flow moves down the radial span. This was the result of two contributing factors. First, that the spanwise velocity component exiting the circumferential cavity is strong at this MFR, as evident by the fact that hot gases have easily traversed the 24 mm and have not been swept significantly downstream by the core flow (less than 10 mm of axial distance). This fact is further confirmed by the HSV image sequence (Figure 8) taken from a top view of the radial vane. This sequence illustrates the temporal variation of the flame migration out of the UCC. The high spanwise velocity was further confirmed by the visualization of the red hot ID endwalls that were observed during testing of MFRs less than 0.1.

The second contributing factor stemmed from the high

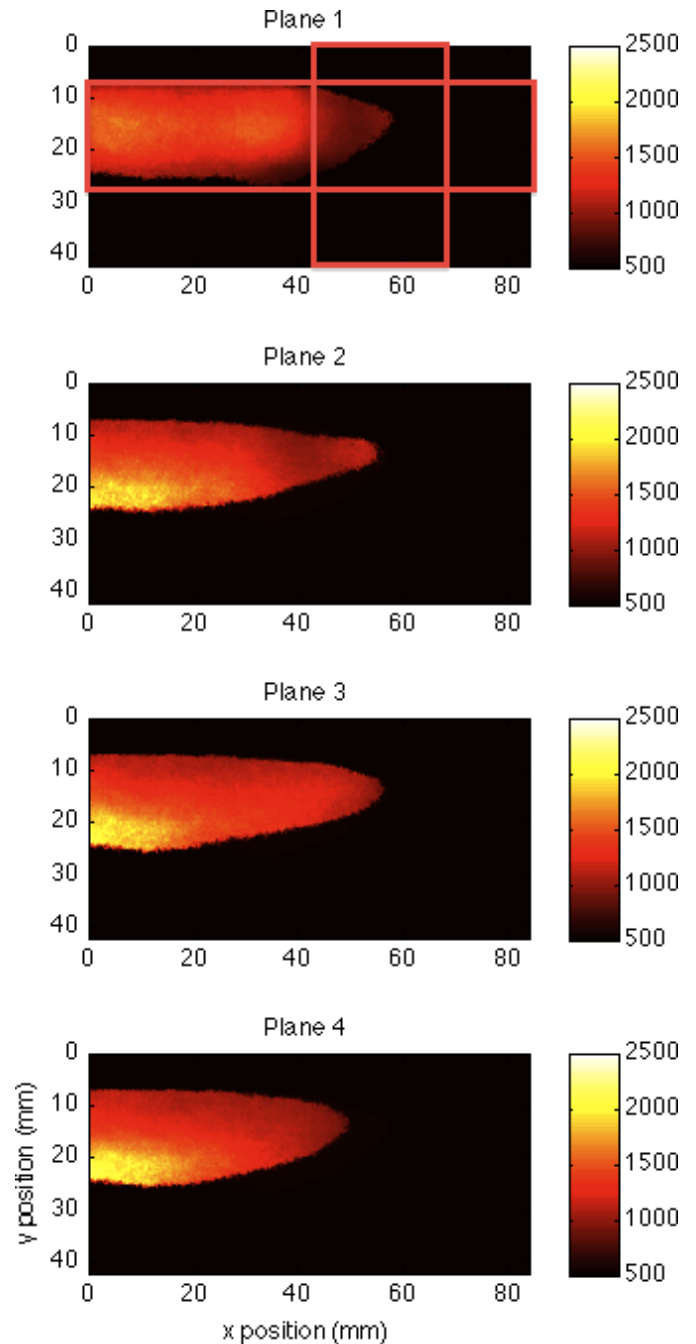


FIGURE 7. Temperature (K) for 28 mm vane, 1000g, MFR=0.2, $\phi = 2.0$ at 6 mm, 12 mm, 18 mm, and 24 mm from Cavity (Test Case 5)

equivalence ratio, $\phi = 2.0$, experienced in At this high ϕ , reacting species were expected to exit the circumferential cavity. Therefore, as these species encountered the core flow, more oxygen was present and the local ϕ dropped towards 1.0. As the reacting species completed combustion at this lower ϕ , the adia-

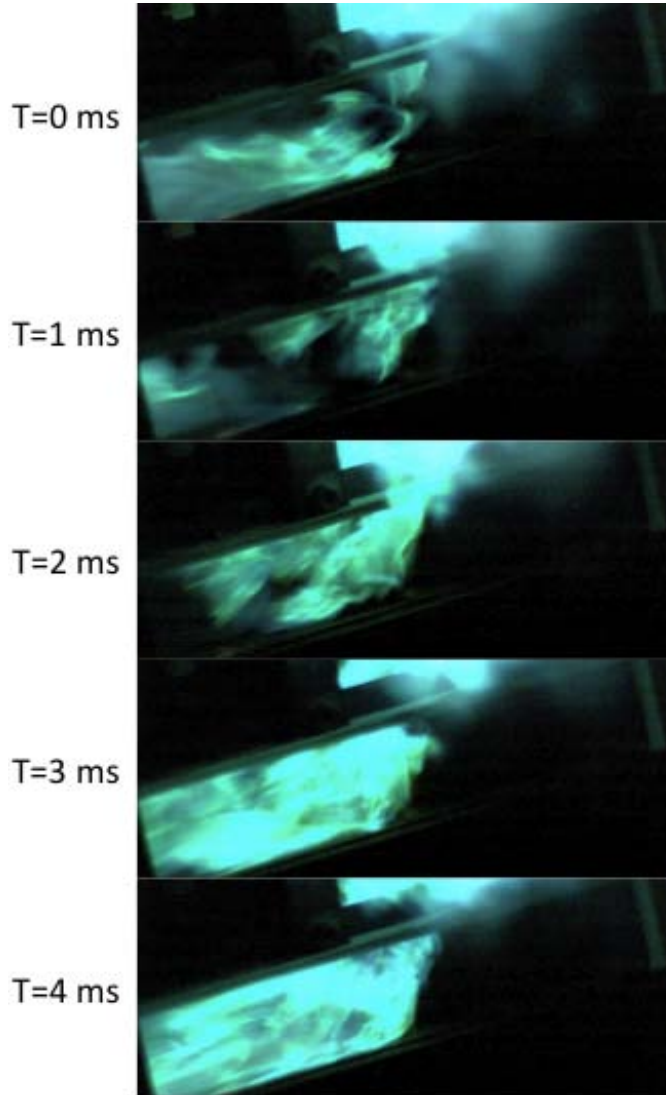


FIGURE 8. High-Speed Video Image Sequence Above Radial Vane of 28 mm vane, 1000g, MFR=0.2, $\phi = 2.0$ (Test Case 5)

batic flame temperature increased. The PLIF data indicated this ϕ reduction as the relative temperature increased down the span and with downstream distance. From this data, exit temperature profiles, taken at $x=0$, were plotted in Figure 9. These profiles represent the pitch-wise temperature distribution at the four radial spans. These profiles are limited by where OH existed in the flow, thus the sharp drop offs in temperature at the edge of the flame ($Y = 7$ and 26 mm). These figures confirm the increase in temperature at the ID span but also suggest that the hottest temperatures are close to the airfoil, but not on the airfoil surface ($Y = 30$ mm). This may however be a ramification that the OH is depleted as the airfoil wall is approached and thus no temperature measurement was recorded.

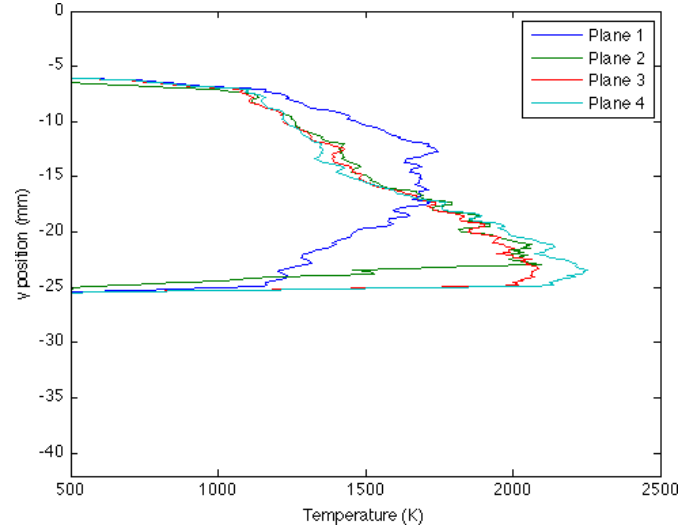


FIGURE 9. Exit Temperature (K) for 28 mm vane, 1000g, MFR=0.2, $\phi = 2.0$ at 6 mm, 12 mm, 18 mm, and 24 mm from Cavity (Test Case 5)

Investigation of Test Cases 4 through 6 revealed the impact of g-loading on the temperature distribution. The higher g-loading was achieved by increasing the flow rate in the UCC cavity as indicated in Table 1. As shown in Figure 10, at 6 mm from the circumferential cavity exit the peak temperature increased with the g-loading. This indicated a faster reaction mechanism as hotter temperatures were achieved at the same location. This could be due to the higher bubble flame velocity as suggested by Lewis [10] at the elevated g-load or simply the higher shear due to the higher velocity ratio at the interface of the UCC and core flows for the same MFR. One note is that at the lowest g-load, Figure 10 suggests that some of the intermediate reacting species were convected slightly upstream of the cavity exit as indicated by the presence of OH ahead of the UCC cavity.

Varying the MFR was accomplished by altering the core flow rates at constant UCC flow rates to maintain the g-loading at the same level. Test Cases 9, 7, 5, and 8, change the core flow by a factor of 6, which represents the realistic range an Ultra Compact Combustor may experience in practice. Figure 11 shows the impact of this variation for the 1000 g-loaded case. From the images at 6 mm from the UCC cavity, it is clearly evident that increasing the core air mass flow significantly increased the post-combustion equilibration rate. Similar results were determined for the other vane heights (not shown). While the ratio of V_{UCC}/V_{core} was actually reduced for the lower MFR, these velocities were still perpendicular to each other and thus, the relative shear between the two flows was expected to increase as the core flow increased. Figure 12 provides the spanwise distribution of the spatially averaged temperatures within the flame region only for a set of images such as those in Figure 7. As evident from this figure, a possible "sweet spot" near MFR=0.2 for the 28 mm

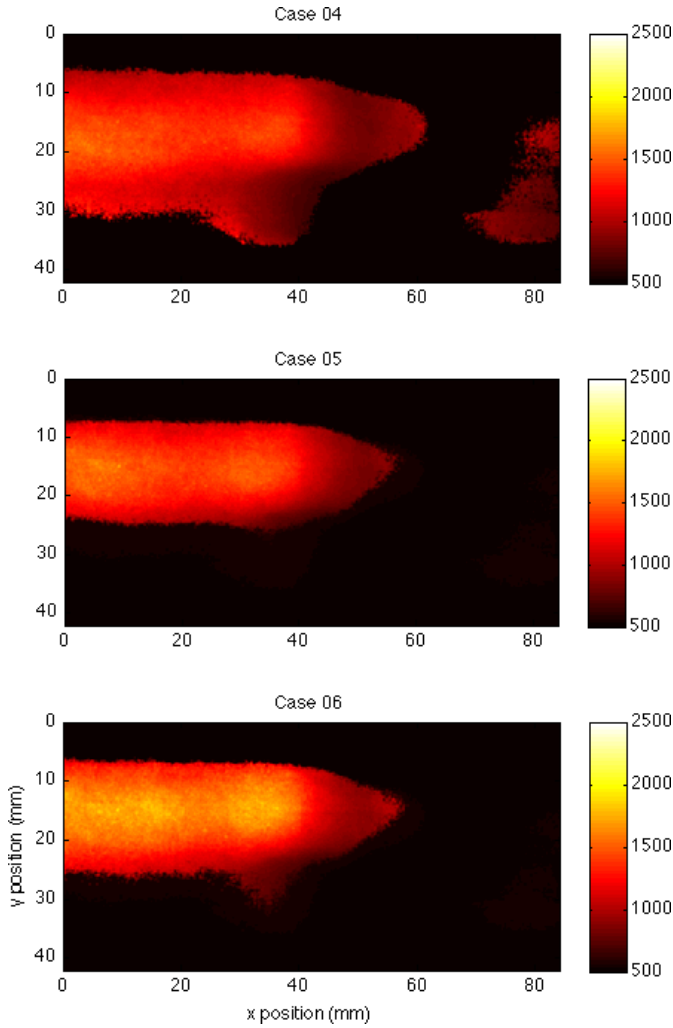


FIGURE 10. Temperature (K) for 28 mm vane, MFR=0.2, $\phi = 2.0$, 6 mm from Cavity, at 500, 1000, and 2000 g's (Test Cases 4, 5, 6)

vane existed that yields a nearly uniform spatially averaged temperature. This is a more ideal exit condition for a typical combustor yielding a turbine exit temperature profile more consistent with typical turbine durability requirements. Potentially more ideal would be a reduction of temperature near the two endwalls which may be occurring in this design, but was not measured by the current four planes.

For the smaller vane height of 14 mm, the ideal MFR increased past 0.3 as evident in Figure 13. Conversely, Figure 14 shows the tallest vane height of 56 mm, which resulted in an ideal MFR closer to 0.1 to achieve a uniform temperature across the span. This is consistent with the concept that the flame more fully fills the core flow channel with the shorter vane. Clearly more core flow was needed to fill and distribute across taller vane heights. Also, the ideal temperature profile seemed to be more a

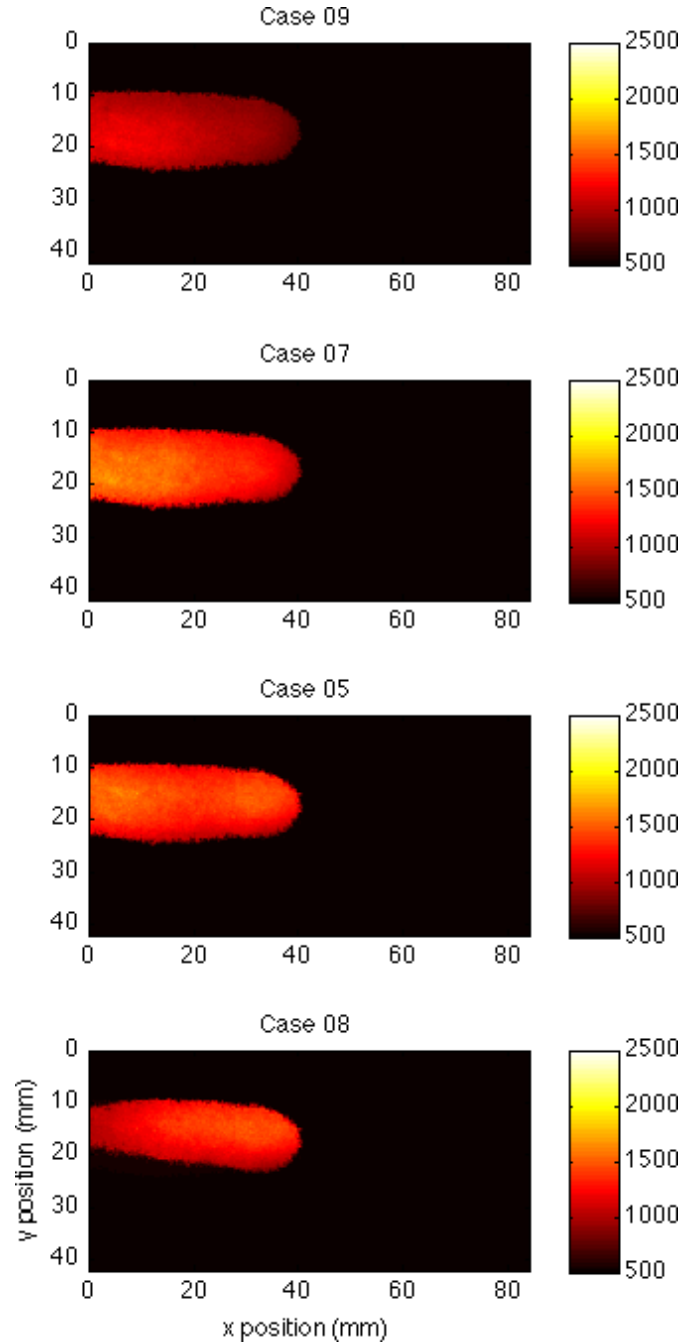


FIGURE 11. Temperature (K) 28 mm vane, 1000g, $\phi = 2.0$, 6 mm from Cavity, at MFR=0.05, 0.1, 0.2, and 0.3 (Test Cases 9, 7, 5, 8)

function of core flow velocity than mass flow rate. For all three vanes, the nominal mean average temperature was around 1150K indicative of the amount of energy to produce a uniform distribution.

Looking specifically at the effect of the vane height, Figures

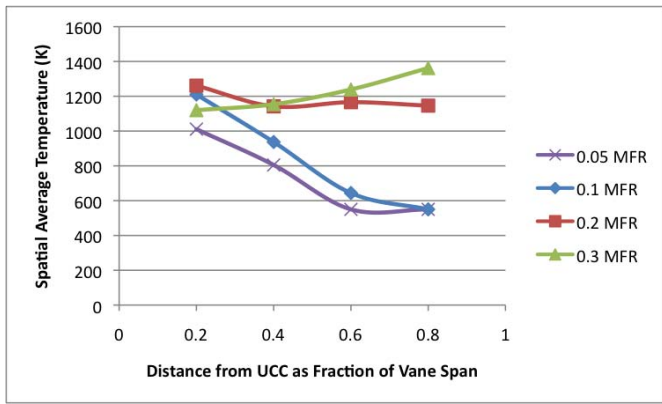


FIGURE 12. Spanwise Spatial Average Temperature of 28 mm vane, 1000g, $\phi = 2.0$ at MFR=0.05, 0.1, 0.2, and 0.3

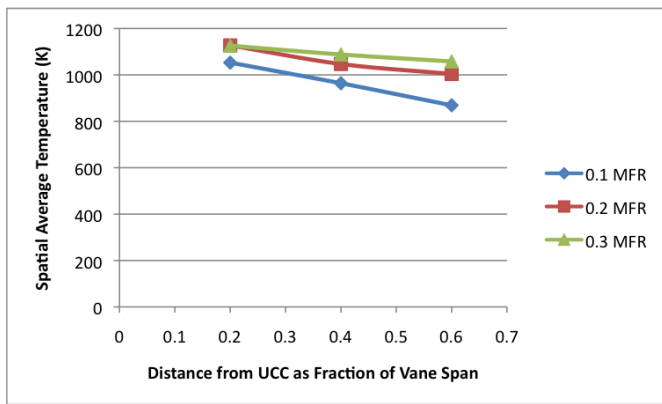


FIGURE 13. Spanwise Spatial Average Temperature of 14 mm vane, 1000g, $\phi = 2.0$ at MFR=0.1, 0.2, and 0.3

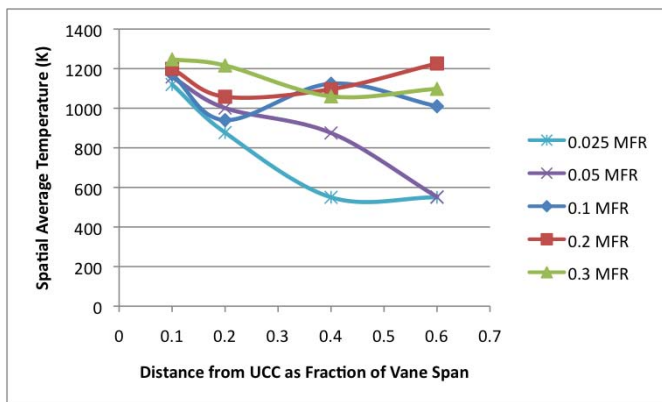


FIGURE 14. Spanwise Spatial Average Temperature (K) of 56 mm vane, 1000g, $\phi = 2.0$ at MFR=0.025, 0.05, 0.1, 0.2, and 0.3

15 and 16 reveal the temperature contours at 1000g and MFR of 0.2 for the 14 mm and 56 mm vanes, respectively. Comparing the results at 6 mm from the UCC for Test Cases 3, 2, and 11, Figures 7a, 15b, 16a respectively showed the vane height significantly altered both the intensity of the combustion process as well as the pitch-wise extent. These three cases all had the same mass flow rates, but at 6 mm from the cavity the smallest vane has a significantly wider flame regime. This was more evident in interrogating the exit temperature profile for these three cases.

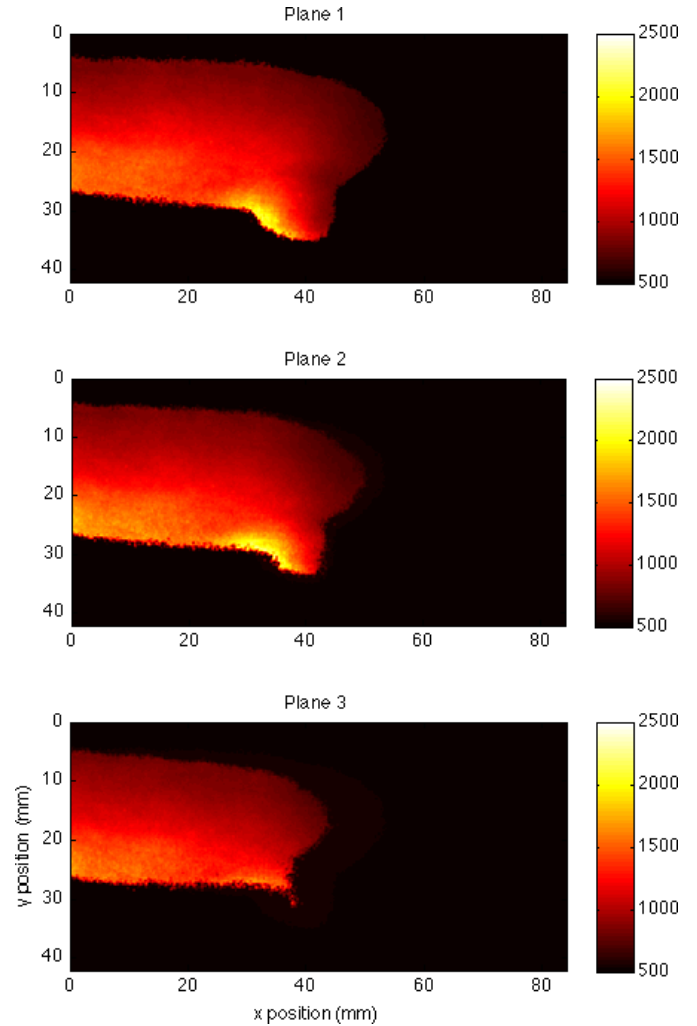


FIGURE 15. Temperature (K) for 14 mm vane, 1000g, MFR=0.2, $\phi = 2.0$ at 3 mm, 6 mm, and 9 mm from Cavity (Test Case 2)

As shown in Figure 17, at this distance from the circumferential cavity, the flame extended nearly 22 mm pitch-wise from the upper wall for the shortest vane, which is the entire height of the channel. This reduced to 18 mm and then 13 mm from the up-

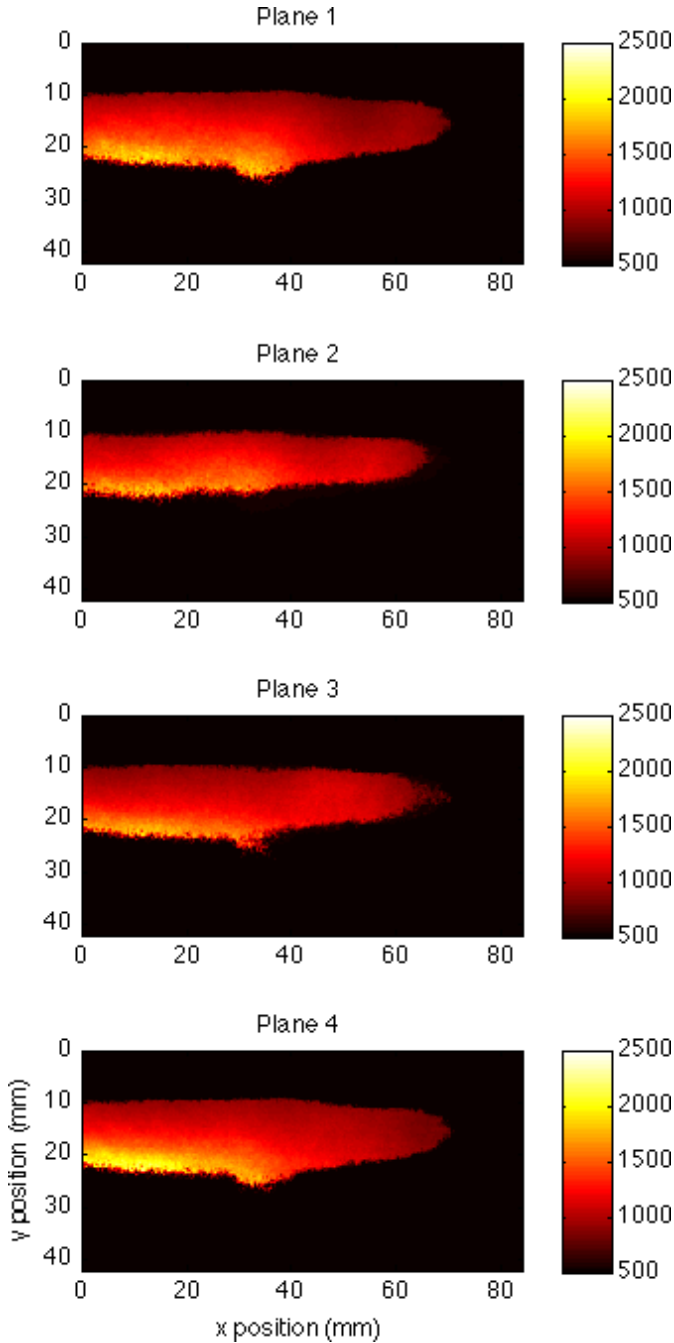


FIGURE 16. Temperature (K) for 56 mm vane, 1000g, MFR=0.2, $\phi = 2.0$ at 6 mm, 12 mm, 24 mm, and 36 mm from Cavity (Test Case 11)

per wall for the 28 mm and 56 mm vane, respectively. This was due to the higher relative UCC flow for the larger vane spans. The flow that exited the UCC from the taller configuration had a higher relative momentum and stayed more cohesive as it entered

the core and continued reacting.

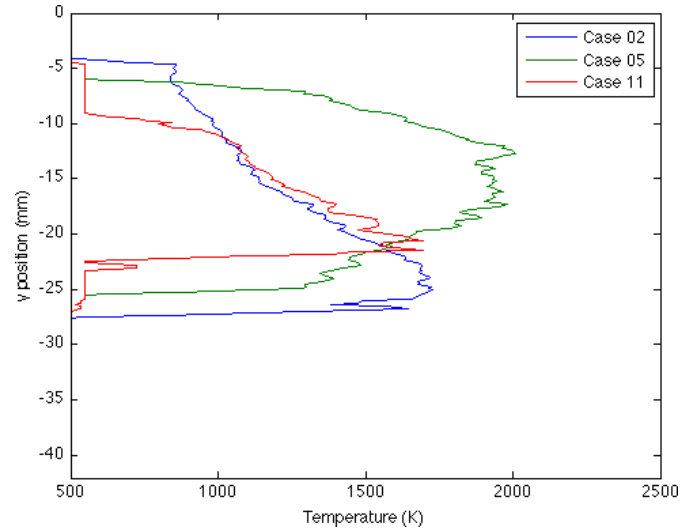


FIGURE 17. Exit Temperature (K) for 1000g, MFR=0.2, $\phi = 2.0$, 6 mm from Cavity, at 14, 28, and 56 mm vanes (Test Cases 2, 5, 11)

One question that arose was whether the radial vane height caused an effect due to the height itself or due to the slowing of the core flow velocity at the same MFR. To investigate this, Test Cases 2, 7, and 13 were run where the core flow was maintained at 13.1 m/s. Figures 18 and 19 provide the temperature distribution in the core flow and the exit profile respectively for these cases. Noticeable was both the significant reduction in the flame width and temperature for the 56 mm vane height. This reduction for the largest vane height was experienced for all spans (not shown). Clearly maintaining the core flow velocity (and velocity ratios) minimized the reaction as the vane height was increased.

Using high-speed video, the injection angle of the flow exiting the UCC and entering the core flow was investigated. Figure 20 shows the trajectory of the flow exiting the UCC for Test Case 5. As illustrated in this figure, the flame injection angle was the measured angle of the flame from the core flow direction.

Similarly to Figure 20, Figure 21 illustrates the flame injection angle for Test Case 7 while Figure 22 shows the same for Test Case 2. Comparing Figure 20 (Test Case 5) with Figure 21 (Test Case 7) for a single vane height with two different core flow velocities yielding an injection angle change from 65.6 to 35.7 degrees. This result was identical for a fixed core mass flow rate over two different vane heights such as Test Cases 5 and 2 (Figures 20 and 22) because the doubling the vane height at the same mass flow rate halved the core flow velocity. However, matching core velocity over two different vane heights (Figures 22 and 21 for Test Cases 2 and 7, respectively) yielded a nearly identical injection angle (35.3 and 35.7 degrees respectively). The results

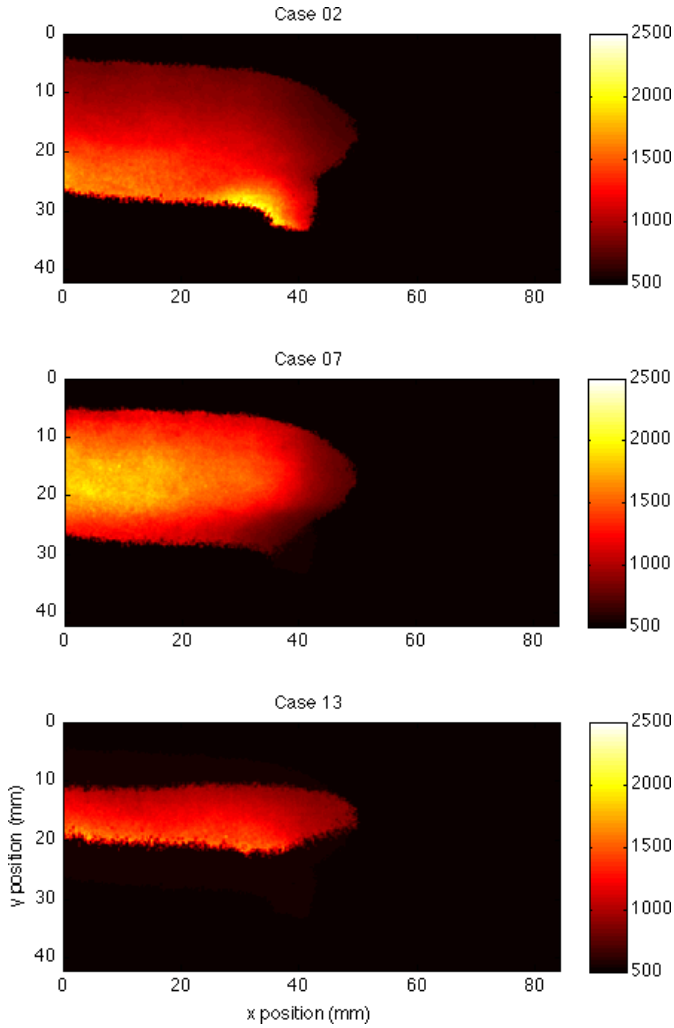


FIGURE 18. Temperature (K) for 1000g, $V_{core} = 13.1\text{m/s}$, $\phi = 2.0$, 6 mm from Cavity, at 14, 28, and 56 mm vanes (Test Cases 2, 7, 13)

were strikingly similar for all vane heights and core flow velocity variations.

Figure 23 quantifies this angle for Test Cases 2, 5, and 11 which represent a constant MFR of 0.2 for the three vane heights while Figure 24 quantifies the variation for Test Cases 2, 7, and 13 which maintain the core velocity at 13.1 m/s for the same vane heights. The flame injection angle was nearly constant at 40 and 60 degrees for the 6.55 m/s and 13.1m/s cases when the velocities (and velocity ratios) were maintained. The 26.2 m/s cases indicate a very loose, at best, relationship between vane height and flame injection angle. These results are expected as the shear was the same for the respective cases, but what was indicated from a migration standpoint was that the intermediate reacting species could not in bulk traverse the entire span of the taller vanes as previously indicated in Figure 18. Maintaining

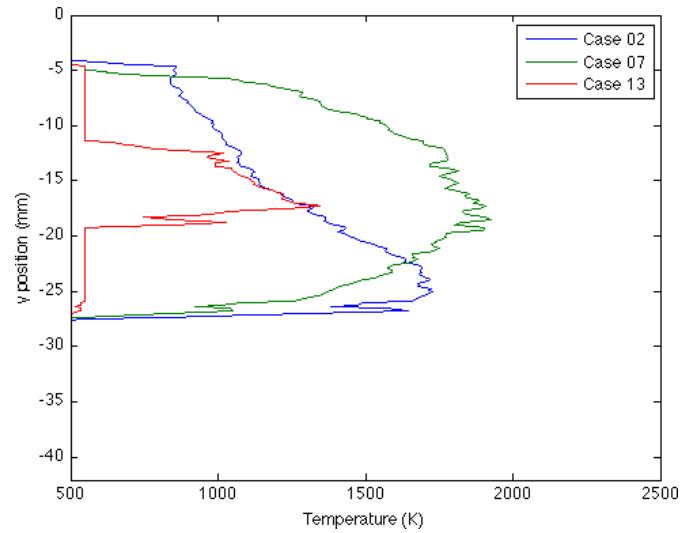


FIGURE 19. Exit Temperature (K) for 1000g, $V_{core} = 13.1\text{m/s}$, $\phi = 2.0$, 6 mm from Cavity, at 14, 28, and 56 mm vanes (Test Cases 2, 7, 13)

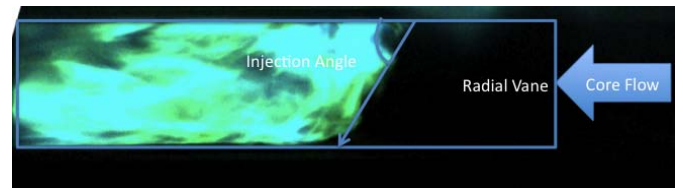


FIGURE 20. High-Speed Video Image Above Radial Vane of 28 mm vane, 1000g, MFR=0.2, $\phi = 2.0$ (Test Case 5)



FIGURE 21. High-Speed Video Image Above Radial Vane of 28 mm vane, 1000g, MFR=0.1, $\phi = 2.0$ (Test Case 7)



FIGURE 22. High-Speed Video Image Above Radial Vane of 14 mm vane, 1000g, MFR=0.2, $\phi = 2.0$ (Test Case 2)

the MRF constant resulted in a sharper injection velocity that was able to fill more of the span of the taller vanes.

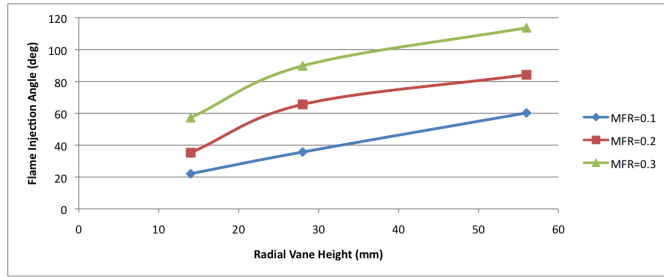


FIGURE 23. Flame Injection Angle from Cavity for 1000g, $\phi = 2.0$, and MFR=0.1, 0.2, 0.3 for each 14, 28, and 56 mm vanes

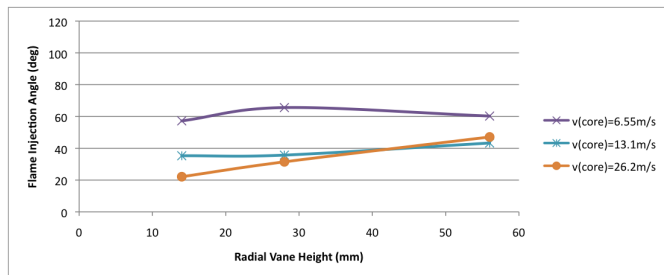


FIGURE 24. Flame Injection Angle from Cavity for 1000g, $\phi = 2.0$, V_{core} =6.55, 13.1, 26.2 m/s for each 14, 28, and 56 mm vanes

CONCLUSION

This study was focused on characterizing the effect of increasing radial vane height on the migration of turbulent g-loaded flames within a sectional model of the UCC. The test rig was constructed to be representative of the full UCC rig currently used by AFRL and to allow optical access for using non-intrusive laser diagnostics. The investigation was centered around using 14, 28, and 56 mm radial vanes in the core flow section while maintaining identical flow conditions for UCC to core air flow ratios, MFR=0.1, 0.2, 0.3. By varying the UCC mass flows the g-load was investigated at 500, 1000, and 2000 g's for the 28mm vane and 1000 g's for the 14 and 56mm vanes. Propane (C_3H_8) was used with a constant equivalence ratio, $\phi = 2.0$ and two-line OH Planar Laser-Induced Fluorescence (PLIF) thermometry was used along side of High-Speed Video (HSV) to investigate the flame migration from the UCC into the core flow above the radial vanes.

This investigation has shown the insight gained from qualitative and quantitative 2-line OH-PLIF thermometry interrogation at the combustor-turbine interface. For the first time, stream-wise, span-wise, and pitch-wise temperature distributions were analyzed at this interface. It was shown that the higher g-load cases (2,5,7) exhibited an "effective" increase in reaction rate as was previously discovered [10, 15]. The pitch-wise flame extension resultant from the pressure gradient of the radial vane cavity was reduced for both higher g-loads, taller radial vane heights,

and lower MFRs. An optimal MFR was suggested for each vane to yield a uniform span-wise exit temperature distribution. This MFR value differed for each vane height as the flame injection angle was a function almost entirely of the core flow velocity and UCC to core flow velocity ratio instead of the mass flow rates. Thus, for a given radial vane height an appropriate injection angle should be chosen to yield the desired exit temperature profile and the core flow velocity adjusted accordingly. However, this may not always be an available option and appropriate design tradeoffs will be necessary. While lower core velocities yielded deeper flame injection into the core flow, the lower velocities also decreased the pressure gradient across the radial vane cavity which reduced its effectiveness.

Further investigations are planned to determine if changes to the velocity flowfield characteristics occur with radial vane height increases. Also, the impact of varying g-loads will be further addressed to include values up to 4000 g's, well past the 3500g threshold of Lewis [10]. Further, changes to the UCC equivalence ratio will be studied particularly at higher core flow velocities to determine if full-span migration can be achieved. Finally, it was observed that the shape of the flame from the UCC's ambient exit changed shape at the lowest UCC to core flow velocity ratios, corresponding to the highest core flow values and this will also be investigated.

ACKNOWLEDGMENT

The authors would like to thank Mr. John Hixenbaugh, for his technical assistance in the lab, and Mr. Jake Schmidt of Spectral Energies, LLC., for his support of our laser diagnostic systems. We would also like to thank Dr. Joe Zelina of AFRL/RZTC for his continued support. This research was sponsored by AFOSR with Dr. Julian Tishkoff as the program manager and AFRL/RZTC.

REFERENCES

- [1] Vogeler, K., 1998. "The potential of sequential combustion for high bypass jet engines". In Int'l Gas Turbine & Aeroengine Congress & Exhibition.
- [2] Sirignano, W. A., and Liu, F., 1999. "Performance increases for gas-turbine engines through combustion inside the turbine". *Journal of Propulsion and Power*, **15**(1).
- [3] Lukachko, S. P., Kirk, D. R., and Waitz, I. A., 2002. "Turbine durability impacts of high fuel-air ratio combustors, part 1: Potential for intra-turbine oxidation of partially-reacted fuel". In ASME Turbo Expo 2002.
- [4] Kirk, D. R., Guenette, G. R., Lukachko, S. P., and Waitz, I. A., 2002. "Gas turbine engine durability impacts of high fuel-air ratio combustors part 2: Near wall reaction effects on film-cooled heat transfer". In ASME Turbo Expo 2002.

- [5] Zelina, J., Sturgess, G. J., and Shouse, D. T., 2004. "The behavior of an ultra-compact combustor (ucc) based on centrifugally enhanced turbulent burning rates". In AIAA.
- [6] Zelina, J., Shouse, D. T., and Hancock, R. D., 2004. "Ultra-compact combustors for advanced gas turbine engines". In ASME Turbo Expo 2004.
- [7] LeBay, K. D., Hankins, T. B., Lakusta, P. J., Branam, R. D., Reeder, M. F., and Kostka, S., 2010. "Oh-plif calibration and investigation within the ultra compact combustor". In AIAA ASM 2010.
- [8] Roquemore, W. M., Shouse, D., Burrus, D., Johnson, A., Cooper, C., and Duncan, B., 2001. "Trapped vortex combustor concept for gas turbine engines". In 39th Aerospace Sciences Meeting & Exhibit, AIAA.
- [9] Yonezawa, Y., Toh, H., Goto, S., and Obata, M., 1990. "Development of the jet-swirl high loading combustor". In 26th Propulsion Conference, AIAA/SAE/ASME/ASME.
- [10] Lewis, G. D., 1973. "Swirling flow combustion – fundamentals and application". In 9th Propulsion Conference, AIAA/SAE.
- [11] Thornburg, H., Sekar, B., Zelina, J., and Greenwood, R., 2007. "Numerical study of an inter-turbine burner (itb) concept with curved radial vane". In 45th Aerospace Sciences Meeting & Exhibit, AIAA.
- [12] Sekar, B., Thornburg, H. J., Briones, A. M., and Zelina, J., 2009. "Effect of trapped vortex combustion with radial vane cavity arrangements on predicted inter-turbine burning performance". In 7th International Energy Conversion Engineering Conference, AIAA.
- [13] Briones, A., Sekar, B., Thornburg, H., and Zelina, J., 2010. "Effect of vane notch and ramp design on the performance of a rectangular inter-turbine burner". In 48th Aerospace Sciences Meeting, AIAA.
- [14] Quaale, R. J., Anthenian, R. A., Zelina, J., and Ehret, J., 2003. "Flow measurements within a high swirl ultra compact combustor for gas turbine engines". In ISABE.
- [15] LeBay, K. D., Drenth, A. C., Thomas, L. M., Polanka, M. D., Branam, R. D., and Schmidt, J. B., 2010. "Characterizing the effects of g-loading in an ultra compact combustor via sectional models". In ASME Turbo Expo 2010.
- [16] Cattolica, R., 1981. "Oh rotational temperature from two-line laser excited fluorescence". *Applied Optics*, **20**.
- [17] Lucht, R. P., Laurendeau, N. M., and Sweeney, D. W., 1981. "Temperature measurement by two-line laser-saturated oh fluorescence in flames". *Applied Optics*, **21**(20), 15 October.
- [18] Seitzman, J. M., Hanson, R. K., DeBarber, P. A., and Hess, C. F., 1994. "Application of quantitative two-line oh planar laser induced fluorescence for temporally resolved planar thermometry in reacting flow". *Applied Optics*, **33**(18), 20 June.
- [19] Meier, U. E., Wolff-Gabmann, D., and Stricker, W., 2000. "Lif imaging and 2d temperature mapping in a model combustor at elevated pressure". *Aerospace Science and Technology*, **4**, 28 March.
- [20] Giezendanner-Thoben, R., Meier, U., Meier, W., Heinze, J., and Aigner, M., 2005. "Phase-locked two-line oh planar laser-induced fluorescence thermometry in a pulsating gas turbine model combustor at atmospheric pressure". *Applied Optics*, **44**(31), 01 November.